Nitrous Oxide for Space Propulsion Applications: Catalytic Decomposition Processes

Rachid Amrousse[1*] and Ahmed Bachar[2]

[1]*JAXA, Japan Aerospace Exploration Agency, 3-1-1 Yoshinodai Chuo-ku, Sagamihara 252-5210 Kanagawa, Japan*

[2]*LMCPA, Laboratoire des Matériaux Céramiques et Procédés Associés, Université de Valenciennes et du Hainaut-Cambrésis, 59300 Valenciennes, France*

Abstact

The completely N_2O decomposition was performed on the substituted $M_xFe_{3-x}O_4$ nanocrystallites (M^{2+} = Ni^{2+} and Mg^{2+} with x = 0–1). The results showed that the partial Fe^{2+} incorporation by Ni^{2+} and Mg^{2+} cations led to a significant improvement in the catalytic activity for the N_2O decomposition. The N_2O conversion reached 100 % over the $Ni_{0.75}Fe_{2.25}O_4$ and $Mg_{0.58}Fe_{2.42}O_4$ catalysts at 533 and 545 K for N_2O (1000 ppm), respectively. A relative increasing of decomposition temperatures was observed after O_2 addition.

Keywords: Decomposition; Nanoparticle; Nitrous oxide; Substituent effects.

* Correspondin author: Rachid Amrousse
Email: rachid.amrousse@jaxa.jp
TEL: +81-50-3362-5956
FAX : +81-42-749-8284

1. Introduction

Nitrous oxide catalytic decomposition has been investigated at Surrey to provide knowledge and experience necessary for the development of the monopropellant microthruster. Previously, several data released that the N_2O catalytic decomposition is feasible for heat and thrust generation [1–3]. On the other hand, N_2O is not only one of the major sources of nitrogen oxides (NO_x) depleting the ozone layer in the stratosphere, but also a strong greenhouse gas with a global warming potential approximately 300 times higher than that of CO_2 [4].

Various types of catalysts have been tested for N_2O catalytic decomposition, such as: Ru/Al_2O_3, Co_3O_4, $Fe_xCe_{1-x}O_2$, $LaCoO_3$, Fe-ZSM-5, and Cu-ZSM-5 [5–10]. Recently, spinel oxides of 3d transition metals have been the subject of increasing fundamental and applied research because of their special electric, magnetic, and catalytic properties [11,12]. It is known that the synthetic process of spinel precursor compounds, which determines final oxide structure, texture, and chemical composition, plays a crucial role in ultimate performance of these spinels [13,14]. Spinel oxides belong to a class of complex oxides with the chemical formulas of AB_2O_4 in which A ions are generally divalent cations occupying tetrahedral sites and B ions are trivalent cations in octahedral sites. The cobalt oxide spinel Co_3O_4, for example, is one receiving considerable interest [15,16]. The A component of the spinel oxide Co_3O_4 is often substituted partially with other divalent 3d transition metals Cr, Mn, Ni, Cu, Zn, and earth alkali metals such as Mg to create special physico-chemical properties for a specific application [11–14]. With regard to their applications in catalysis, for example, it has been known that the catalytic activity of these spinels depends essentially on two factors: the degree of A substitution and the degree of inversion of the spinel. These two material parameters in turn depend heavily on the synthetic approach and post synthesis treatment of the precursor compounds [13–17].

He Hong group also reported that the introduction of CeO_2 into the Co_3O_4 spinel could promote the catalytic activity [18]. Moreover, it is well known that cobalt-based catalysts present excellent catalytic activities for N_2O decomposition [19–23]. Different strategies for N_2O abatement have been recently suggested [24]. Among those solutions, catalytic processes for the decomposition of N_2O into N_2 and oxygen are usually considered as an attractive way but usually suffer from poisoning effects at low temperature due to strong adsorptions of O_2 and water [25–27].

The present work focuses to the preparation, characterization and evaluation of partial substituted magnetite which was highly active for N_2O decomposition into nitrogen and oxygen, even in the presence of excess oxygen.

2. Experimental

2.1. Catalyst preparation

The $Ni_xFe_{3-x}O_4$ magnetite samples were prepared via solid-state reaction as described in [28]. The precursors prepared by sufficiently grinding the mixture of ferrous sulfate heptahydrate $FeSO_4 \cdot 7H_2O$, sodium hydroxide NaOH, different amounts of Nickel Sulfate hexahydrate $NiSO_4 \cdot 6H_2O$ and dispersant at room temperature were calcined at 1000 K. Moreover, one series of spinel nanocrystalline $Mg_xFe_{3-x}O_4$ catalysts were synthesized via a highly exothermic and self–sustaining reaction named solution combustion synthesis method or SCS [29]. Especially, a concentrated aqueous solution of various precursors (metal nitrates and urea) was located in an oven at 900 K in air for 20 minutes to decompose the very fast reaction. Under these conditions, nucleation of metal oxide crystals is induced, their growth is limited and nano-sized grains can be obtained.

Two different preparation methods were selected to ensure the synthesis of $Ni_xFe_{3-x}O_4$ and $Mg_xFe_{3-x}O_4$ nanoparticles.

2.2. Catalyst characterization

Synthesized Fe_3O_4 and partially $M_xFe_{3-x}O_4$ (M^{2+} = Ni^{2+} and Mg^{2+}) nanocrystalline frameworks were analyzed by XRD (X-ray diffraction); mass 200 mg of finely ground powder was placed in a holder standard sample. The XRD patterns were recorded with Cu-K_α radiation; $\lambda_{Cu\ K\alpha}$ = 1.5406 Å; over a 2θ range of 10–70°. The specific surface area was obtained through N_2 adsorption-desorption measurements at 77 K and analysis of the adsorption data by the BET model using a ASAP^{TM} 2020 accelerated surface area and porosimetry system: 4 h pretreatment at 500 K under nitrogen flow; N_2 in He with $P(N_2)$ = 0.3 bar. The single point data were obtained at P/P_o value of 0.3. The composition of the catalysts was determined by AAS with a WFX–10 atomic absorption spectrometer. The experimental temperature programming reduction (TPR) was carried out at a heating rate of 10 K min^{-1}, up to 963 K. The amount of expending H_2 was measured using a thermal conductivity detector. Particle size and morphology of nanocrystalline magnetites were determined via transmission electron microscopy (TEM) using an accelerating voltage of 200 kV. Moreover, the nanoparticles were first dispersed in anhydrous ethanol by ultrasonication, and then the suspension was dropwise deposited onto a copper grid, coated with carbon films, and dried in

air naturally. The temperature-programmed desorption with oxygen (TPD-O_2) method was used; 50 mL min^{-1} as flow of 10 vol. % O_2 diluted in He; and was carried out in ''MicroVision 2 TPD'' apparatus coupled by on-line mass spectrometer analyzer. Before starting TPD-O_2 run, the samples were activated under flowing O_2 + He mixture at 400 °C for 90 min.

2.3. Catalyst decomposition tests

The decomposition of nitrous oxide results in formation of nitrogen and oxygen according to the following reaction equation:

$N_2O(g) \rightarrow N_2 + ½O_2(g) + Heat$

At standard conditions this exothermic reaction generates ~ 82 kJ of heat per mole of N_2O [30,31]. However, heat input is required to initiate the reaction. In the case of thermal decomposition, the activation energy barrier for N_2O is about 250 kJ mol^{-1} [31]. Therefore, in order to achieve the required reaction rates, the gas must be heated to above 1273 K. The N_2O catalytic decomposition were performed on a microthruster by valve opening of gas mixture of N_2O (1000 ppm) or N_2O (1000 ppm) + 10 vol. % O_2 mixtures in a preheated catalytic fixed-bed as shown in our previous study [33].

The gas flows of mixtures were passed into a He flow rate (100 mL min^{-1}) over 400 mg of catalyst to get a space velocity GHSV (Gas Hourly Space Velocity) of 20 000 h^{-1}, the decomposition reaction was followed by temperature sensors and pressure sensors placed in the upstream and the downstream of the reactor. Before catalytic tests, the catalytic bed reactor was preheated at 673 K for 2 h by He + 10 vol. % O_2 mixture to eliminate impurities: organic compounds adsorbed on the catalytic surface, then the temperature was decreased. To reach a reasonable N_2O catalytic conversion, the reaction system was carried out at each temperature process for 45 minutes, then started to analyze ejected gas by on-line gas chromatograph (GC–MS–2010 chromatograph) equipped with molecular sieve 5 Å and Porapak Q columns and TCD detector (SRI 310 CG). Method of fragment masses m/z was used to identify the nature of each possible ejected gas (e.g. N_2O, NO, NO_2, N_2 and O_2 fragments). The N_2O conversions were determined by analyzing N_2O feed concentrations before (bypass) and after passing through the catalyst bed.

3. Results and discussion

3.1. Catalyst characterization

Characterization results of prepared nanocrystalline samples with different amounts of Fe^{2+} substituted by Ni^{2+} and Mg^{2+} cations are shown in Table 1.

Table 1. Surface area, pore volume and pore diameter of partially substituted $M_xFe_{3-x}O_4$ framework.

Catalysts	Surface area ($m^2\ g^{-1}$)	Porous volume ($cm^3\ g^{-1}$)	Pore diameter (nm)
Fe_3O_4	52	0.08	64
$Ni_{0.21}Fe_{2.79}O_4$	107	0.34	110
$Ni_{0.58}Fe_{2.42}O_4$	124	0.38	125
$Ni_{0.75}Fe_{2.25}O_4$	131	0.42	142
$Ni_{0.92}Fe_{2.08}O_4$	67	0.29	127
$NiFe_2O_4$	55	0.11	94
$Mg_{0.21}Fe_{2.79}O_4$	92	0.28	88
$Mg_{0.58}Fe_{2.42}O_4$	111	0.31	113
$Mg_{0.75}Fe_{2.25}O_4$	119	0.31	128
$Mg_{0.92}Fe_{2.08}O_4$	88	0.25	115
$MgFe_2O_4$	53	0.14	172

The obtained results show that the specific surface area of materials increased heavily from 52 to 131 $m^2\ g^{-1}$ after substitution of x = 0.75 of Fe^{2+} by Ni^{2+} and from 52 to 119 $m^2\ g^{-1}$ after replacement of x = 0.58 by Mg^{2+}. Accordingly, the BET surface area decreased when more Fe^{2+} substituted by Ni^{2+} and Mg^{2+} loadings.

Generally, XRD can be used to characterize the crystallinity of nanoparticles, and it gives an average diameter of all the nanoparticles. The XRD patterns of the Fe_3O_4 and partially substituted $Ni_xFe_{3-x}O_4$ (x = 0.75 and 1) nanoparticle samples are shown in Fig. 1 (A).

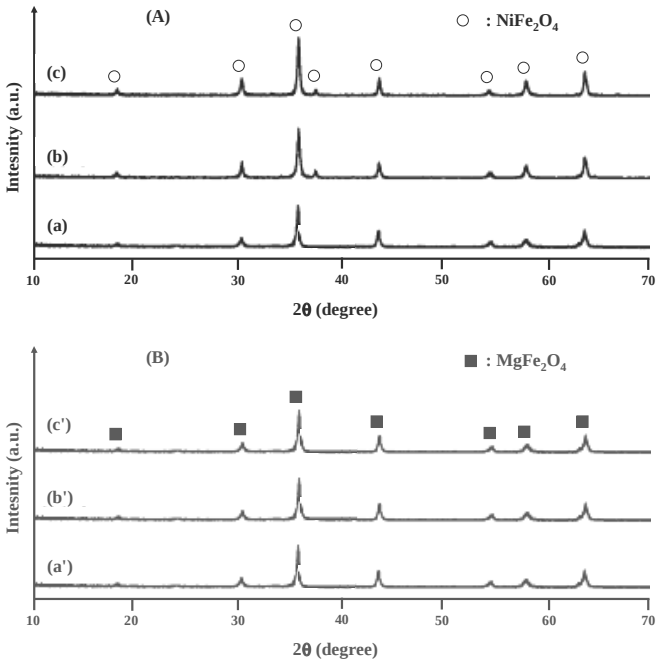

Figure 1. (A): XRD patterns of: (a) Fe_3O_4 spinel, (b) substituted $Ni_{0.75}Fe_{2.25}O_4$ and (c) $NiFe_2O_4$ magnetite samples. (B): XRD patterns of: (a') Fe_3O_4 spinel, (b') substituted $Mg_{0.58}Fe_{2.42}O_4$ and (c') $MgFe_2O_4$ magnetite samples.

The discernible peaks can be indexed to (220), (311), (400), (422), (511) and (440) planes of a cubic unit cell, which corresponds to that of magnetite structure. Furthermore, the characteristic peaks can be indexed as the cubic structure $NiFe_2O_4$ (pattern (c)), which is accorded with the reported data (JCPDS card 74–2081). The reflected peaks confirm that a good crystalline $NiFe_2O_4$ powder had been synthesized under these conditions. The lattice parameters a = b = c = 8.331 Å estimated from XRD pattern are close to the reported results of 8.337 Å (JCPDS card 74–2081). The peaks with 2θ values of 30.1; 35.6; 37.2; 43.2; 53.6; 57.2; 62.8 and 74.3° correspond to the crystal planes (220), (311), (222), (400), (422), (511), (440), (533) of nanocrystalline $NiFe_2O_4$, respectively. Moreover, the reflectance peak (311) became more intense than the other peaks after Ni^{2+} incorporation into Fe_3O_4; this indicates that crystallization of particles has taken place along the easy direction (311) of $NiFe_2O_4$.

The XRD pattern of the $MgFe_2O_4$ nanocrystallites is shown in Fig. 1. (B). The XRD analysis confirmed the formation of single-phase $MgFe_2O_4$ cubic spinel, showing well defined reflection of allowed planes. The $MgFe_2O_4$ is accorded to the reported data (JCPDS card 8–1935). The crystallite size of all samples is calculated using Scherrer's relation [32]. Thus, XRD patterns of partial substituted $Ni_{0.75}Fe_{2.25}O_4$ nanocrystalline show a slight increase of peak intensities after incorporation of Ni^{2+} into Fe_3O_4, this might be related to an interaction Ni–Fe.

In order to check the morphology and mean crystallite size, the synthesized nanocrystalline samples were analyzed by TEM Microscopy.

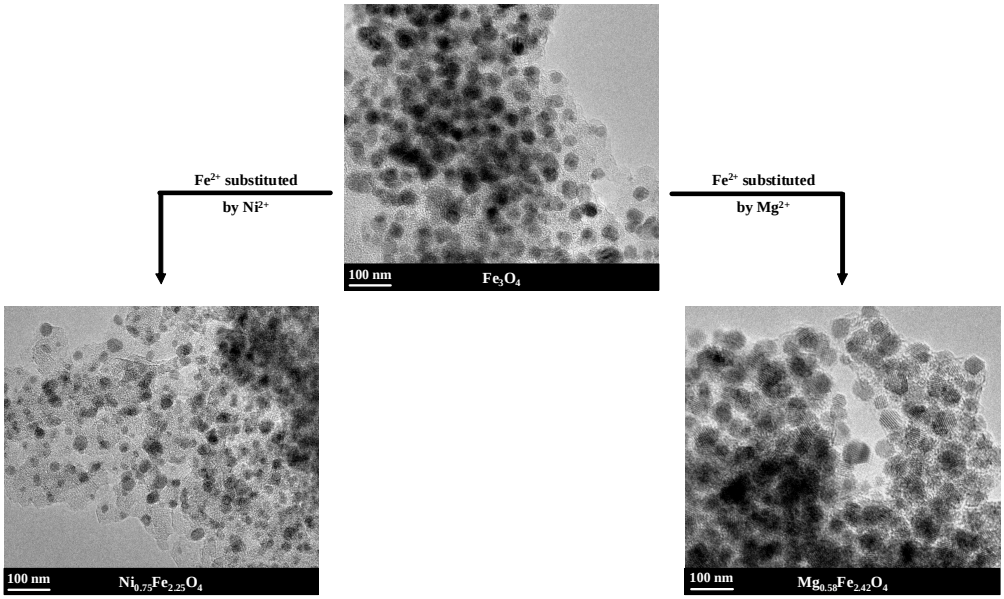

Figure 2. TEM micrographs of nanocrystalline Fe_3O_4, partially substituted $Ni_{0.75}Fe_{2.25}O_4$ and partially substituted $Mg_{0.58}Fe_{2.42}O_4$ magnetite frameworks.

Fig. 2 shows the TEM micrographs of Fe_3O_4, $Ni_{0.75}Fe_{2.25}O_4$ and $Mg_{0.58}Fe_{2.42}O_4$ nanocrystalline spinels. As can be seen, low particle size dispersion is detected with mean sizes within the estimated values by Debye Scherrer equation with XRD data. Thus, the closeness between the estimated XRD and TEM sizes indicates the single crystalline structure of nanoparticles.

Table 2. Nanoparticle sizes of Fe_3O_4 and partially substituted $M_xFe_{3-x}O_4$ (M^{2+} = Ni^{2+} and Mg^{2+}) frameworks.

Samples	d_{XRD}	d_{TEM}
Fe_3O_4	57	52
$Ni_{0.75}Fe_{2.25}O_4$	41	38
$Mg_{0.58}Fe_{2.42}O_4$	64	55

Table 2 presents the obtained results of average particle sizes, which is in agreement with data obtained from TEM images.

Otherwise, the incorporation of Ni^{2+} cation into Fe_3O_4 structure allows for much smaller particle sizes. The average size was similar when the Fe^{2+} substituted by Mg^{2+} cation. The $M_xFe_{3-x}O_4$ nanocrystallite sizes were changed after incorporation of Ni^{2+} and Mg^{2+} cations into Fe_3O_4 structure. In fact, in substituted $M_xFe_{3-x}O_4$ structures, the larger crystal radius Fe^{2+} (0.77 Å) is replaced by smaller ionic crystal radius Ni^{2+} (0.69 Å) and similar ionic crystal radius Mg^{2+} (~ Fe^{2+} ≈ 0.75 Å), respectively.

TPR profiles of Fe_3O_4, $Ni_{0.75}Fe_{2.25}O_4$ and $Mg_{0.58}Fe_{2.42}O_4$ are displayed in Fig. 3.

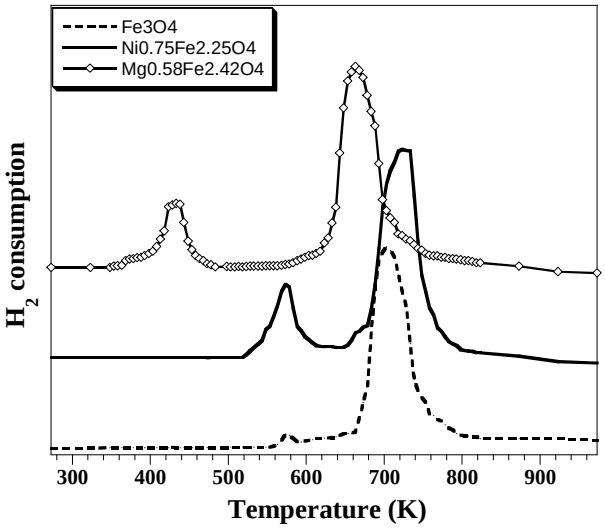

Figure 3. TPR profiles of Fe_3O_4, $Ni_{0.75}Fe_{2.25}Fe_2O_4$ and $Mg_{0.58}Fe_{2.42}O_4$ magnetite samples.

The strong TPR peak appeared at 693 K of Fe_3O_4 reduction. The typical hydrogen reduction profiles present the two-stage reductions which have been reported by other workers [34–36]. A small peak at around 573 K was due to the reduction of Fe_2O_3 to Fe_3O_4:

$3Fe_2O_3 + H_2 \rightarrow 2Fe_3O_4 + H_2O$ Eq. (1)

The peaks whose maxima were located about 710 K were due to the second reduction step from Fe_3O_4 to the metallic iron:

$Fe_3O_4 + 4H_2 \rightarrow 3Fe + 4H_2O$ Eq. (2)

Obviously, the different substituted magnetite frameworks exhibit the different TPR profiles, where both $Ni_{0.75}Fe_{2.25}O_4$ and $Mg_{0.58}Fe_{2.42}O_4$ give two peaks. For both samples, mostly two reduction peaks are observed. From the relative intensity of both peaks it can be assumed that they correspond respectively to Mg (Ni) and Fe_3O_4 reduction at high temperatures, although that there is no clear cut between both processes, this result was in agreement with literature [37]. However, the first H_2-TPR peak of $Ni_{0.75}Fe_{2.25}O_4$ shows a sharp reduction of NiO. However, the first H_2-TPR peak in the case of $Mg_{0.58}Fe_{2.42}O_4$ sample corresponds to the reduction of Fe_2O_3 to Fe_3O_4 explained by Eq. (1). This reduction step was shifted to low temperature may be caused by the interaction Mg–Fe.

On the other hand, the second sharp peak corresponds to the reduction step from Fe_3O_4 to Fe^0 as explained by Eq. (2).

Moreover, pure Fe_3O_4 and partially substituted $Ni_{0.75}Fe_{2.25}O_4$ and $Mg_{0.58}Fe_{2.42}O_4$ samples were analyzed with TPD-O_2 desorption.

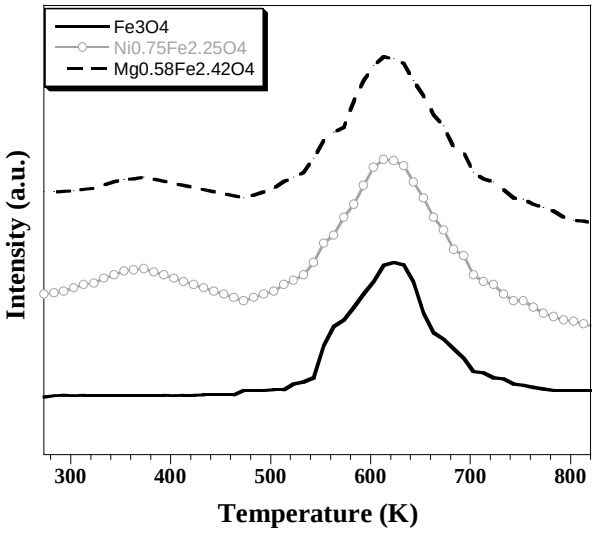

Figure 4. TPD profiles of O_2-desorption over pure Fe_3O_4 and partially substituted $Ni_{0.75}Fe_{2.25}O_4$ and $Mg_{0.58}Fe_{2.42}O_4$ samples.

Fig. 4 presents the corresponding O_2-desorption peaks: (i) at 624 K over Fe_3O_4 ferrite, (ii) a lower signal at low temperatures (273–473 K) and (303–464 K) over $Ni_{0.75}Fe_{2.25}O_4$ and $Mg_{0.58}Fe_{2.42}O_4$ catalysts, respectively.

Wherefore, the inhibition difference of O_2 on the catalytic performances of studied samples was confirmed, indicating that when the temperature increased, O_2 was desorbed from the active sites of catalysts. In fact, the N_2O decomposition can be represented by an anionic redox mechanism.

3.2. N_2O Catalytic decomposition process

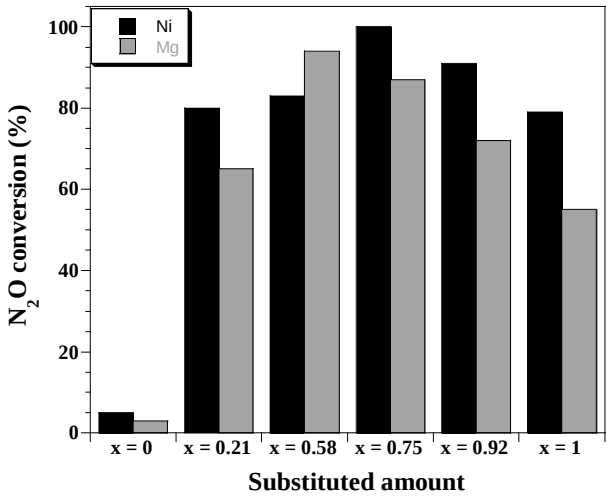

Figure 5. N_2O (1000 ppm) conversion to N_2 and O_2 gaseous phase at 533 K over Fe_3O_4 magnetite with different degree of substituted Ni^{2+} and Mg^{2+} cations.

Fig. 5 shows N_2O catalytic conversion results over different partially substituted $M_xFe_{3-x}O_4$ catalysts at 533 K. It showed that the partial substitution of Fe^{2+} by both Ni^{2+} and Mg^{2+} cations has significantly promoted the catalytic performance for N_2O (1000 ppm) decomposition into N_2 and O_2, the N_2O catalytic decomposition performed at atmospheric pressure in He flow with a space velocity GHSV = 20 000 h^{-1}. For $Ni_xFe_{3-x}O_4$ samples, N_2O conversion increased sorely from 5 to 80 % when the Ni^{2+} amount increased from x = 0 to x = 0.21, then smoothly increased to 100 % as maximum conversion at x = 0.75. When x = 1, the catalytic activity for N_2O decomposition relatively decreased. Moreover, the substituted $Mg_xFe_{3-x}O_4$ spinels were thereabouts similar to $Ni_xFe_{3-x}O_4$ samples when Mg^{2+} amount increased from x = 0 to x = 0.58. However, the $Mg_xFe_{3-x}O_4$ prepared catalysts showed the uppermost activity at x = 0.58, then the catalytic activity progressively decreased with a maximum of Mg^{2+} amount (x > 0.58). Our previous study reported in [38] presents the substitution effect on N_2O catalytic decomposition over $Mg_xFe_{3-x}O_4$ (M^{2+} = Ni^{2+} and Mg^{2+}) spinels in a flow open regime. However, their results showed that the substituted Fe_3O_4

magnetite catalysts were more actives for N_2O decomposition than that of pure Fe_3O_4 sample. The difference in catalytic activity for N_2O decomposition is due to the synthesis process and post treatment of the precursors.

We can summarize that the catalytic activity of the partially $Ni_xFe_{3-x}O_4$ and $Mg_xFe_{3-x}O_4$ catalysts depended highly on the substituted amount of Fe^{2+} by Ni^{2+} and Mg^{2+} cations. When the partial substitution of Fe^{2+} cation was different, the best amount was x = 0.75 of Ni^{2+} and x = 0.58 of Mg^{2+}.

The catalytic activities of substituted magnetites; in which Fe^{2+} was almost replaced by Ni^{2+} and Mg^{2+} amounts, were less than that with partial substitution. Indeed, the existence of Ni^{2+} or Mg^{2+} in magnetite frameworks might have a deep effect with Fe^{2+} to form best active sites of N_2O catalytic decomposition. Indeed, Fe^{2+} in Fe_3O_4 serves as the active site for the catalytic N_2O decomposition. Therefore, Fe^{2+} is also the adsorption site for O_2 species after the N_2O decomposition. When, the amounts x = 0.75 of Ni^{2+} or x = 0.58 of Mg^{2+} were incorporated into Fe_3O_4, the O_2–desorption from the active sites is facilitated. Finally, when more Ni^{2+} or Mg^{2+} (x = 1) were added, an interaction Ni–Fe or Mg–Fe and the increase of surface area led to a significant improvement in the catalytic activity for the N_2O decomposition. Therefore, these results have identified the substituted magnetite $M_xFe_{3-x}O_4$ frameworks are widely active than pure magnetite.

As cited bellow, the N_2O decomposition can be explained by an anionic redox mechanism process initiated by the oxygen-atom transfer. Whereas for tested catalysts, the anionic redox mechanism is expected with the principal steps [39]:

$N_2O_{(g)} + O^{2-}{}_{surf} \rightarrow O_2{}^{2-}{}_{surf} + N_{2(g)}$

(N–O bond breaking via O_2 transfer) Eq. (3)

$O_2{}^{2-}{}_{surf} + O_2{}^{2-}{}_{surf} \rightarrow 2O^{2-}{}_{surf} + O_{2(g)}$ (O_2 recombination) Eq. (4)

In this case, the recombination of $O_2{}^{2-}{}_{surf}$ to produced final $O_{2(g)}$ occurs according to Eq. (4). Obviously, some other possible variants of the oxygen migration and recombination steps are also possible invoking the same species.

3.3. Addition effect of O_2 on N_2O decomposition

The addition of 10 vol. % O_2 often inhibited the N_2O decomposition reaction.

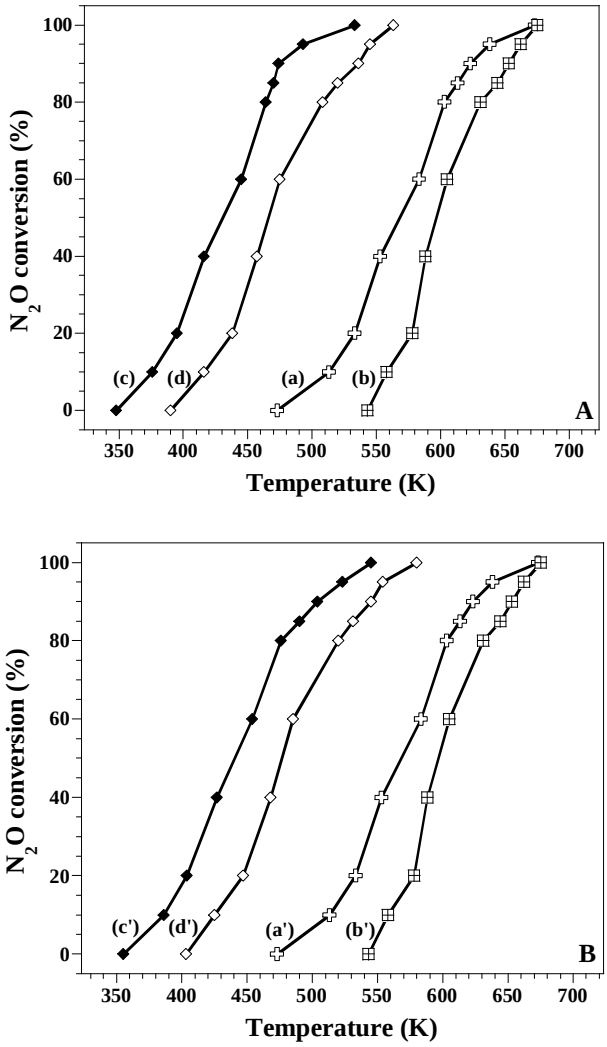

Figure 6. (A): N_2O catalytic conversion in different feed compositions: (a) N_2O (1000 ppm) and (b) N_2O (1000 ppm) + 10 vol. % O_2 over Fe_3O_4; (c) N_2O (1000 ppm) and (d) N_2O (1000 ppm) + 10 vol. % O_2 over $Ni_{0.75}Fe_{2.25}O_4$ catalysts. (B): N_2O catalytic conversion in different feed compositions: (a') N_2O (1000 ppm) and (b') N_2O (1000 ppm) + 10 vol. % O_2 over Fe_3O_4; (c') N_2O (1000 ppm) and (d') N_2O (1000 ppm) + 10 vol. % O_2 over $Mg_{0.58}Fe_{2.42}O_4$ samples.

Fig. 6 presents N_2O conversion for reaction systems at different temperatures over Fe_3O_4, $Ni_{0.75}Fe_{2.25}O_4$ and $Mg_{0.58}Fe_{2.42}O_4$ synthesized catalysts.

Although pure Fe_3O_4 magnetite had very low activity in the present work of N_2O catalytic decomposition, indicating that high conversion was obtained at high temperature, the incorporation of Ni^{2+} and Mg^{2+} into the spinel Fe_3O_4 frameworks led to significant expansion in catalytic performance for N_2O decomposition, indicating that high conversion was obtained at low temperature, making the N_2O conversion shift ~ 180 K to lower temperatures. The addition of 10 vol. % O_2 inhibited the N_2O decomposition reaction, which desired that oxygen flow decelerate the N_2O adsorption into the active sites after gaseous competition. The inhibition procedure of O_2 for N_2O decomposition over $Ni_{0.75}Fe_{2.25}O_4$ catalyst is lower than

that over $Mg_{0.58}Fe_{2.42}O_4$, indicating that the adsorption of O_2 on $Mg_{0.58}Fe_{2.42}O_4$ catalyst is hard than that on $Ni_{0.75}Fe_{2.25}O_4$ catalyst.

3.4. Space velocity and its effect on N_2O catalytic decomposition behavior

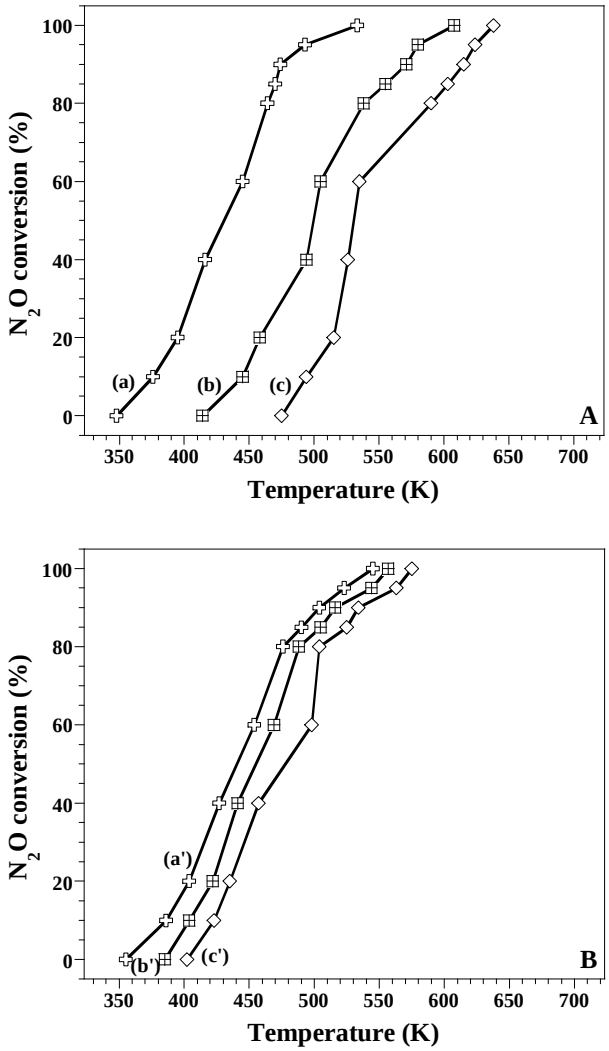

Figure 7. (A): N_2O (1000 ppm) conversion over $Ni_{0.75}Fe_{2.25}O_4$ at different GHSV: (a) 20 000 h^{-1}, (b) 30 000 h^{-1} and (c) 40 000 h^{-1}. (B): N_2O (1000 ppm) conversion over $Mg_{0.58}Fe_{2.42}O_4$ at different GHSV: (a') 20 000 h^{-1}, (b') 30 000 h^{-1} and (c') 40 000 h^{-1}.

Fig. 7 gives the GHSV effect on the N_2O conversion at different temperatures over substituted $Ni_{0.75}Fe_{2.25}O_4$ and $Mg_{0.52}Fe_{2.48}O_4$ samples. Both figures showed that the N_2O catalytic conversion shifted to higher temperature versus high space velocity. The N_2O conversion reached 20 % (i.e. in chemical regime) over $Ni_{0.75}Fe_{2.25}O_4$ at 395; 458 and 515 K at 20 000; 30 000 and 40 000 h^{-1} GHSV, respectively. Although the conversion achieved 20 % in the presence of $Mg_{0.58}Fe_{2.42}O_4$ at 404; 442 and 435 K for same GHSV values indicated previously.

Conclusion

The obtained results have revealed that the incorporation of Ni^{2+} and Mg^{2+} cations into Fe_3O_4 spinel frameworks significantly promoted the catalytic activity of N_2O decomposition. The catalytic activity of partially $M_xFe_{3-x}O_4$ (M^{2+} = Ni^{2+} and Mg^{2+}) spinel frameworks depended on the amount of Fe^{2+} substitution. Moreover, partial substituted samples present the best behavior in the N_2O catalytic decomposition, the conversion of N_2O decomposition to N_2 and O_2 reached 100 % at lower temperature in comparison with N_2O decomposition over pure Fe_3O_4 magnetite. Although the addition of molecular oxygen to the feed gases inhibited the N_2O decomposition reaction, N_2O can also be decomposed completely to N_2 and O_2 at 563 and 580 K in the presence of 10 vol. % O_2 over $Ni_{0.75}Fe_{2.25}O_4$ and $Mg_{0.58}Fe_{2.42}O_4$, respectively.

Acknowledgements

The authors acknowledge financial support from Japan Aerospace Exploration Agency (JAXA).

References

[1] V.A. Zakirov, T.J. Lawrence, J.J. Sellers, M.N. Sweeting, Proceedings of the 5th International Symposium on Small Satellite Systems and Services, France, **2000**.

[2] V.A. Zakirov, V. Goeman, T.J. Lawrence, M.N. Sweeting, Proceedings of the 14th Annual AIAA/USU Conference on Small Satellites, the United States, **2000**.

[3] V.A. Zakirov, T.J. Lawrence, J.J. Sellers, M.N. Sweeting, Proceedings of the 51st International Astronautical Congress, Rio de Janeiro, Brazil, **2000**.

[4] J. Peréz–Ramírez, F. Kapteijn, G. Mul, X.D. Xu, J.A. Moulijn, Catal. Today, **2002**, *76*, 55–74.

[5] V.G. Komvokis, M. Marti, A. Delimitis, I.A. Vasalos, K.S. Triantafyllidis, Appl. Catal. B, **2011**, *103*, 62–71.

[6] E. Wilczkowska, K. Krawczyk, J. Petryk, J.W. Sobczak, Z. Kaszkur, Appl. Catal. A, **2010**, *389*, 165–172.

[7] F.J. Perez-Alonso, I. Melian-Cabrera, M.L. Granados, F. Kapteijn, J.L.G. Fierro, J. Catal. **2006**, *239*, 340–346.

[8] J.P. Dacquin, C. Lancelot, C. Dujardin, P. Da Costa, G. Djega-Mariadassou, P. Beaunier, S. Kaliaguine, S. Vaudreuil, S. Royer, P. Granger, Appl. Catal. B, **2009**, *91*, 596–604.

[9] J. Peréz-Ramírez, F. Kapteijn, G. Mul, J.A. Moulijn, Chem. Commun. **2001**, 693–694.

[10] P.T. Fanson, M.W. Stradt, J. Lauterbach, W.N. Delgass, Appl. Catal. B, **2002**, *38*, 331–347.

[11] R. Sundararajan, V. Srinivasan, Appl. Catal. **1991**, *73*, 165–171.

[12] Y. Liang, R. Tong, W. Xiaolai, J. Dong, S. Jishuan, Appl. Catal. B, **2003**, *45*, 85–90.

[13] L. Markov, A. Lyubchova, J. Mater. Sci. Lett. **1991**, *10*, 512–514.

[14] M. Qian, H.C. Zeng, J. Mater. Chem. **1997**, *7*, 493–499.

[15] M. Oku, Y. Sato, Appl. Surf. Sci. **1992**, *55*, 37–41.

[16] Z.P. Xu, H.C. Zeng, J. Mater. Chem. **1998**, *8*, 2499–2506.

[17] U. Chellam, Z.P. Xu, H.C. Zeng, Chem. Mater. **2000**, *12*, 650–658.

[18] L. Xue, C.B. Zhang, H. He, Y. Teraoka, Appl. Catal. B, **2007**, *75*, 167–174.

[19] M. Haneda, Y. Kintaichi, H. Hamada, Appl. Catal. B, **2005**, *55*, 169–175.

[20] K. Asano, C. Ohnishi, S. Iwamoto, Y. Shioya, M. Inoue, Appl. Catal. B, **2008**, *78*, 242–249.

[21] C. Ohnishi, K. Asano, S. Iwamoto, K. Chikama, M. Inoue, Catal. Today **2007**, *120*, 145–150.

[22] F. Zasada, P. Stelmachowski, G. Maniak, J.-F. Paul, A. Kotarba, Z. Sojka, Catal. Lett. **2009**, *127*, 126–131.

[23] P. Stelmachowski, G. Maniak, A. Kotarba, Z. Sojka, Catal. Commun. **2009**, *10*, 1062–1065.

[24] J. Peréz-Ramírez, F. Kapteijn, K. Schöffel, J.A. Moulijn, Appl. Catal. B, **2003**, *44*, 117–151.

[25] G. Centi, L. Dall'Olio, S. Perathoner, J. Catal. **2000**, *192*, 224–235.

[26] G. Centi, L. Dall'Olio, S. Perathoner, J. Catal. **2000**, *194*, 130–139.

[27] V. Boissel, S. Tahir, C.A. Koh, Appl. Catal. B, **2006**, *64*, 234–242.

[38] Z. Zhang, Y. Liu, G. Yao, G. Zu, Y. Hao, Int. J. Appl. Ceram. Technol. (2012), doi: 10.1111/j.1744-7402.2011.02719.x.

[29] N. Russo, D. Fino, G. Saracco, V. Specchia, J. Catal. **2005**, *229*, 459–469.

[30] Lide D.R., CRC Handbook of Chemistry and Physics, 76th Ed. CRC Press. David R. Lide Editor in Chief, Inc., **1995**.

[31] P.W. Atkins, L.L. Jones, Chemistry: Molecules, Matter and Change, 3rd Ed., W. H. Freeman and Company, New York, **1997**.

[32] R. Amrousse, A. Tsutsumi, A. Bachar, D. Lahcene, Appl. Catal. A, **2013**, *450*, 253–260.

[33] P. Sivakumar, R. Ramesh, A. Ramanand, S. Ponnusamy, C. Muthamizhchelvan, Mater. Lett. **2011**, *9*, 1438–1440.

[34] A. Lycourghiotis, D. Vattis, React. Kinet. Catal. Lett. **1981**, *18*, 377–380.

[35] A.J. Kock, H.M. Fortuin, J.W. Gecis, J. Catal. **1985**, *96*, 261–275.

[36] I.R. Leith, M.G. Howden, Appl. Catal. **1988**, *37*, 75–92.

[37] E. Manova, T. Tsoncheva, D. Paneva, J.L. Rehspringer, K. Tenchev, I. Mitov, L. Petrov, Appl. Catal. A, **2007**, *317*, 34–42.

[38] R. Amrousse, T. Katsumi, Catal. Commun. **2012**, *26*, 194–198.

[39] P. Stelmachowski, F. Zasada, W. Piskorz, A. Kotarba, J.F. Paul, Z. Sojka, Catal. Today, **2008,** *137*, 423–428.